Optical Self-Organization in Bulk and Multiquantum Well GaAlAs Microresonators

R. Kuszelewicz, I. Ganne, I. Sagnes, and G. Slekys
Laboratoire Concepts et Dispositifs pour la Photonique, URA250 CNET/CNRS, B.P. 107, 92225, Bagneux cedex, France

M. Brambilla
Dipartimento di Fisica e Istituto Nazionale di Fisica della Materia Politecnico di Bari, Bari, Italy
(Received 17 September 1999)

We have observed optical patterns in GaAs/GaAlAs vertical-cavity microresonators. Rolls, rhombs, or hexagons were obtained depending on the wavelength detuning. We show that cavity thickness fluctuations contribute to pattern selection.

PACS numbers: 42.65.Sf, 42.65.Tg, 47.54.+r, 68.65.+g

In the last decade extensive work has been carried out in the field of transverse nonlinear optics, motivated by the possibility of observing optical self-organization such as spatial solitons or global optical patterns. These structures arise from the interplay of nonlinear light propagation with transverse mechanisms such as light diffraction or transverse diffusion of excited states [1]. A serious difficulty for achieving self-organization is the intrinsic lack of stability of solitons propagating in a space with a number of transverse dimensions greater than one. In order to circumvent this fundamental limitation, specific systems based on nonlinear resonators have been proposed, taking into account transverse diffractive and possibly diffusive mechanisms. This has introduced the phenomenology necessary for describing patterned or localized optical states in cavities, among which cavity solitons (CS) [2–4] are a very appealing class. There, the cavity feedback is a key mechanism to stabilize localized state. As for experiments, solitons have been evidenced in macroscopic resonators [5,6]. The self-confining properties of CS make them candidates for storing and processing all-optical information bits, especially in controlled and reconfigurable optical arrays [3]. This self-organization not only allows self-pixellation of processor arrays, or alternative and elegant solutions to addressing problems at high packing densities, but also proposes quite innovative processing schemes including, e.g., operative modes of the cellular automaton type [7].

In optical information processing and more particularly in optoelectronics and telecommunication, III-V semiconductor microresonators offer a wide range of functional applications such as sources, amplifiers, modulators, and bistable memory elements. This is for a large part due to the combination of micrometer-scale integration, large material flexibility, and intrinsic stability of their geometrical properties. At the same time, recent modeling schemes have introduced direct gap semiconductors as candidate materials for realizing the active part of a nonlinear microresonator. In particular, the main (heavy hole) excitonic line displays nonlinearities analogous to that of an atomic two-level system [8], while, below the band gap, the Urbach's tail can be represented by a simple model of saturable refractive index [9] displaying a negative dispersive nonlinearity. These models showed that a modulational instability (MI) of the homogeneous input-output curve causes the formation of global patterns and stable CS. In these systems, the patterns are intimately linked to CS, and the observation of the former can be considered as an intermediate milestone in the quest for the latter [4].

In this Letter, we report experimental observations of periodic optical patterns in a passive nonlinear resonator. These observations were performed by use of a monolithic microresonator structure with characteristic longitudinal dimensions on the micrometer scale and by exploiting the variety of linear and nonlinear optical properties of III-V semiconductors. Two samples—A and B—grown by metalorganic vapor-phase epitaxy technique (MOVPE) were used. They share a common basic structure consisting of a back mirror made of 23.5 pairs of a $Ga_{0.9}Al_{0.1}As/AlAs$ alternation of quarter-wave layers, a front mirror comprising 17 pairs of the same alternation, and the active layer between the two mirrors. The active layer of sample A comprises a nonlinear multi-quantum-well (MQW) layer including 18 GaAs wells of 100 Å thickness separated by 100 Å -thick $Ga_{0.7}Al_{0.3}As$ barriers. The gap of the MQWs was determined by photoluminescence and found at 849 nm. The cavity resonance was tuned to $\lambda = 875$ nm. In sample B the active part is a simple $3\lambda/2$-thick GaAs layer whose gap is at 872 nm. The cavity resonance is set at 900 nm. Because of the growth conditions, the samples display both short-range thickness fluctuations translating into interface roughness at the atomic level, and a long-range deterministic thickness gradient. Our experiments show a marked sensitivity to thickness fluctuations even on the scale of a single atomic layer, due to the large finesse of these devices.

The excitation scheme took into account that the beam should be much larger than the diffraction length $a = \sqrt{\lambda \mathcal{L} \mathcal{F}/2\pi^2}$ that defines a transverse length scale, where $\mathcal{L}$ is the active layer thickness, λ is the excitation wavelength, and $\mathcal{F}$ the cavity finesse. The cavity finesse of our samples lies in the range 500–800, and consequently the diffraction length is typically 4.5 μm. Thus the beam

 0031-9007/00/84(26)/6006(4)$15.00

diameter was set to 60 μm. The experimental setup uses an argon-ion-pumped CW titanium-sapphire laser source. The near infrared linearly polarized Gaussian beam is then modulated by an acoustooptic modulator generating triangular or rectangular pulses whose duration is limited to 4 μs in order to avoid thermal effects. A polarizing beam splitter (PBS) and a quarter-wave plate (QWP) are used to separate the incident and the reflected beams. The incident beam is focused at normal incidence onto the sample through a 8× microscope objective. The reflected beam is detected in parallel by two different sensors: a Si avalanche photodiode (Si-APD) measures the intensity of the reflected beam and compares it to a reference in order to determine the transient reflectivity, while a charge-coupled device (CCD) camera resolves spatially the time-averaged transverse distribution of light of the near field imaged onto it.

Samples were studied in a regime corresponding to an almost purely saturable defocusing nonlinearity. The intensity levels of the rectangular pulses allowed setting the system to arbitrary biases with respect to the switching point. We thus polarized sample A below threshold. As the laser was tuned towards the cavity resonance, the reflected beam acquired a spatial structure exhibiting increasing contrast and regularity. It should be stressed that, at fixed frequency, these patterns could be observed at arbitrarily low intensities [Fig. 1(a)], i.e., no observable transition between a homogeneous and a patterned response could be detected. These patterns seem to appear without any instability threshold, their contrast fading together with the decrease of intensity of the input beam. When increasing the intensity beyond the plane wave bistability threshold [10], instead, the beam center switches into a low reflectivity state while the peripheral part (still below bistability threshold) retains the original patterns [Fig. 1(b)]. Therefore these patterns arise from a MI in the high reflectivity branch.

Various patterns were observed, depending on the cavity detuning from resonance, but also on the precise part of the sample we used. Because of the wedged thickness of the sample, the position of the laser spot on it determines the spectral position of the Fabry-Perot resonance. Figure 2 shows three patterns observed for different positions on samples A and B and excitation wavelengths. Different patterns have been observed, with their geometry evolving continuously as a function of the cavity detuning, from stripelike to quasirhomboidal or from rhombs to quasihexagons. As the detuning is decreased (in absolute value) towards resonance, the nonlinear interaction due to the increasing intracavity intensity tends to promote a pattern with a higher degree of symmetry.

The spatial fluctuations of layer thickness appear to be a determining factor in the stability of optical patterns. By translating the sample in the transverse plane under a fixed incident Gaussian beam, the patterns move together with the sample irrespective to the boundary conditions imposed by the beam. In our opinion, the predominance of thickness fluctuations over beam boundary conditions in fixing spatially the optical patterns comes from the conjunction of (1) a MI on the high reflectivity branch of the input-output characteristics (2) the absence of a threshold for these MI. This prevents the existence of a sharp switching front that would act as a strong boundary condition imposed by the field on the formation of patterns. Because the beam diameter is much larger than the diffusion and diffraction lengths, the phenomena observed can be analyzed within plane wave framework. This approach is also supported by the observation of pattern formation throughout the beam profile, as a consequence of the absence of an MI threshold: in a plane wave model there are no intensity contours at finite distance that can impose a strong boundary condition to patterns. Therefore, in the following, we shall adopt the model of Spinelli *et al.* [8], regardless of the Gaussian profile of the incident beam.

While a thorough theoretical interpretation of the observations presented so far is the subject of a further publication, we report here some results obtained by adapting the models of [8,11] to our structures. We analyzed the behavior of distributed-Bragg-reflector (DBR) microresonators based on MQW and bulk active layers under off-resonance conditions and found no qualitative difference between them. Therefore we illustrate here results relative to the simpler MQW model which describe the nonlinear coupling to the material by means of an effective two-level

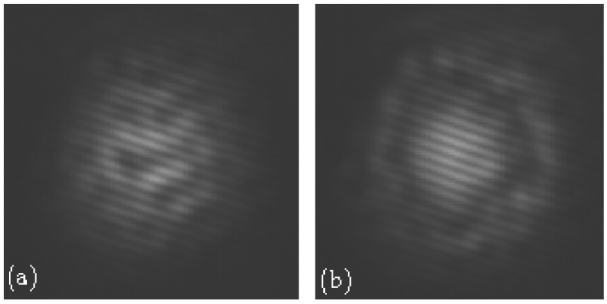

FIG. 1. (a) Irregular pattern generated by the modulational instability of the high reflectance branch of a 60 μm diameter Gaussian beam, incident on sample A at 879.11 nm. At higher (b) intensities, spatial switching brings the center of the beam to a lower reflectivity state, leaving the outer part of the beam in its patterned state.

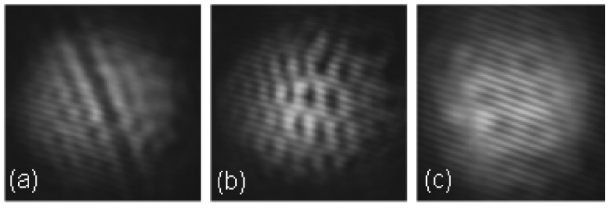

FIG. 2. Images of patterns of various geometrical characteristics on sample A: (a) rolls at 875.68 nm and (b) rhombs at 875.70 nm; and sample B: (c) hexagons at 906.27 nm.

transition. The dynamics of the intracavity field and of the carrier density include paraxial diffraction and diffusion. The equations can be cast in the form [8]:

$$\frac{\partial E}{\partial t} = -(1 + i\theta)E + E_I + 2Ci\,\frac{1 - i\Delta}{1 + \Delta^2}\,(N - 1)E + i\nabla_\perp^2 E\,, \quad (1)$$

$$\frac{\partial N}{\partial t} = -\gamma[N + \beta N^2 + |E|^2(N - 1) - d\nabla_\perp^2 N]. \quad (2)$$

The quantities E, E_I, and N are the normalized profiles of the intracavity and injected fields and carrier density, respectively. Time and spatial variables have been scaled to the cavity linewidth κ and diffraction length a, respectively, $\theta = (\omega_{\rm cav} - \omega_l)/\kappa$ is the normalized cavity detuning, γ is the normalized carrier recombination, Δ is the detuning of the band-gap edge from laser frequency, β is the carrier pair recombination rate, and $d = l_D^2/a^2$ is the scaled diffusion coefficient. The parameter C is proportional to the nonlinear absorption coefficient. Diffraction and diffusion are described by the transverse Laplacian operator $\nabla_\perp^2 \equiv \partial^2/\partial x^2 + \partial^2/\partial y^2$.

We chose a parameter set compatible with the measured quantities and verified the behavior, of the deterministic MI in the high reflectivity branch of the bistable stationary curve. As can be seen on Fig. 3, a MI affects a sizable region of the lower excitation branch. Some preliminary simulations showed that the pattern can "follow" the sample when the medium's dynamics enslaves the field's, while for fast media this phenomenon does not appear. Mostly, we have concentrated on the mechanism responsible for the sensitivity of MI threshold on the fluctuations of the cavity resonance frequency. The dominant systematic source of inhomogeneities in epitaxial samples originates from monolayer-thick (~3 Å) interface steps [12]. As the number of interfaces is around 100, the local thickness of a resonator is a particular realization of some random variable, which results in a local Fabry-Perot resonance frequency becoming a random function of position in the transverse plane, i.e., $\omega_{\rm cav}(\vec{r}) = \overline{\omega}_{\rm cav}[1 + \varepsilon q(\vec{r})]$ where $\overline{\omega}_{\rm cav}$ is now the mean resonance frequency, $\varepsilon = \delta\omega/\overline{\omega}_{\rm cav}$ is the mean fluctuation, $\vec{r} = (x, y)$ and $q(\vec{r})$ is a normally distributed random function whose correlation length l_c defines the typical dimension of transverse uniformity, and has a spectral distribution $\tilde{q}(\vec{K})$. Then the random detuning $\theta = \overline{\theta}[1 + \eta q(\vec{r})]$ is introduced in the model equations (1) and (2). For any variable $X \equiv E, E^*$, or N, with stationary value X_S, the spatiotemporal stability is studied by analyzing the behavior of small perturbations to such solutions of the form $X(t, \vec{r}) = X_S + x(t, \vec{r})$, where the perturbation for the field and the carriers ($x \equiv e, e^*$ or n) has the spatiotemporal expansion $x(t, \vec{r}) = \int \tilde{x}(\vec{K}) \exp[i\vec{K}\vec{r} + \lambda(\vec{K})t]\, d\vec{K}$, introducing the modulation wave vectors $\vec{K}$ and the Lyapounov coefficients $\lambda(\vec{K})$. Standard techniques yield the equation of the field fluctuation component $e(\vec{K})$ as

$$\lambda(\vec{K})\tilde{e}(\vec{K}) = -(1 + i\overline{\theta})\tilde{e}(\vec{K}) - i\overline{\theta}\eta \int d\vec{k}\, \tilde{q}(\vec{K})\tilde{e}(\vec{K} - \vec{k}) + 2Ci(1 - i\Delta)/(1 + \Delta^2) \times [E_S\tilde{n}(\vec{K}) + (N_S - 1)\tilde{e}(\vec{K})] - iK^2\tilde{e}(\vec{K})\,. \quad (3)$$

The two other equations for $\tilde{e}^*(\vec{K})$ and $\tilde{n}(\vec{K})$ have a similar form. The second term in the right-hand side of Eq. (3), scatters the field component $\tilde{e}(\vec{K} - \vec{k})$ to the other $\tilde{e}(\vec{K})$, via the component $\tilde{q}(\vec{K})$ of disorder. This is reminiscent of the mechanism of erosion of a band-gap edge due to the presence of structural disorder in a crystal [13]. In a similar way, this mechanism can relax the sharp MI threshold so that patterns can appear at a lower intensity. The relaxation of the MI threshold is controlled by the spectral properties of the distribution $q(\vec{r})$ which has its peak at $|\vec{K}_{fl}| = 2\pi/l_c$. Its relative values with respect to the wave vector at MI threshold determines the efficiency of the scattering mechanism.

It is beyond the scope of this paper to solve the analytical problem raised by these fluctuations. However, an extended trail of analyses and simulations has been performed, including the Gaussian beam profile and the stochastic process $q(\vec{r})$ with parameters apt to meet the typical features of the actual layer fluctuations. Ranges for noise strengths and correlation lengths have been kept between $\eta = 1$, corresponding to a mean fluctuation of one linewidth, and $\eta = 5$, our typical evaluation for the current samples. While this work is still in progress it is already clear that correlated fluctuations can significantly

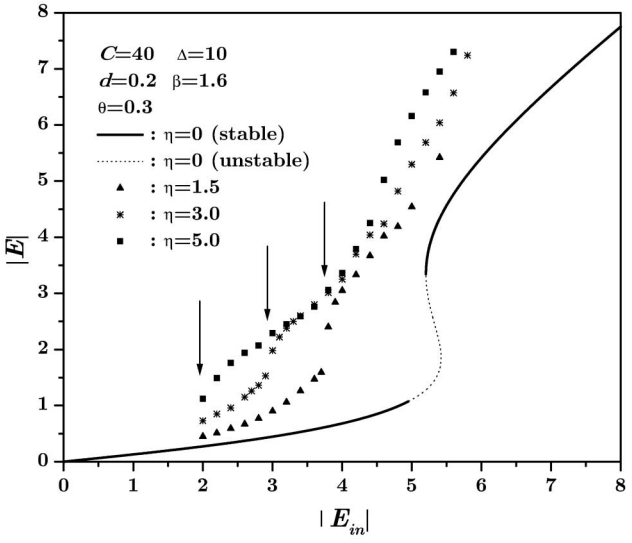

FIG. 3. The homogeneous input-output field curve for a device similar to sample A (line). The broken line is the unstable portion of the curve. The points result from simulations that include the thickness fluctuations with different amplitudes and mark the maximum intensity of a noisy pattern. Arrows mark the intensity of the transition to a self-organized structure.

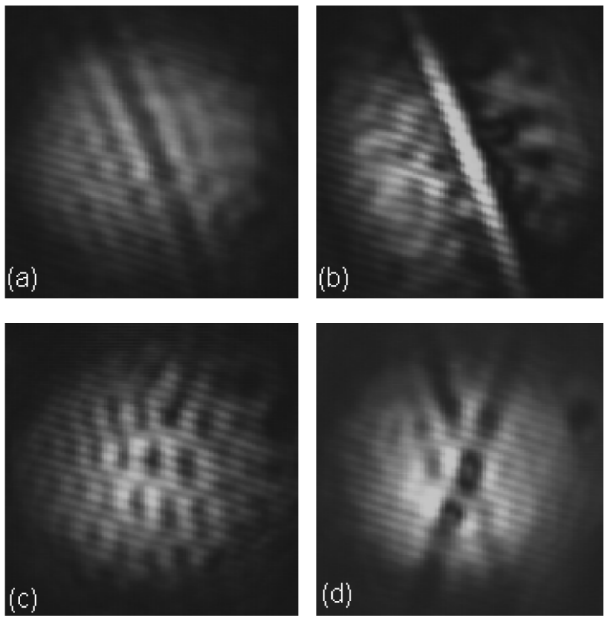

FIG. 4. Moving the excitation wavelength up to the resonance value reveals material structure defects on which self-organized patterns nucleate. Rolls: (a) 875.57 nm, (b) 875.81 nm; rhombs: (c) 875.62 nm; (d) 875.96 nm.

lower the MI threshold. Figure 3 shows three input-output curves for increasing values of the noise strength. The points correspond to the maximum intensity of the pattern observed in the transmitted beam. The steep part of the curves corresponds to a transition towards a self-organized pattern which occurs for injected intensities lower than that of the homogeneous case. Although the calculated patterns are not periodic, the amplitude of the transition seems to decrease correlatively with the decrease of the threshold in a manner reminiscent of the experimental behavior. Experimental measurements of the correlation length obtained by evaluating near resonance the average size of dark regions—at resonance—and bright regions—out of resonance—showed that this length is smaller than the resolution of our optical imaging system, i.e., 1 μm. If one compares it to the typical value of pattern periodicity (10 μm), one sees that our experiments lie in a strong scattering regime.

Pattern shapes may even be more strongly induced by localized material or structural defects. Figure 4a (4b) shows how the striped (rhomboidal) patterns shown in Fig. 2a (2b) are generated by two crossed linear defects. These defects are revealed when, as in Fig. 4, the field is closer to resonance than in Fig. 2, where no defects are visible. Finally, no defects were detectable under the patterns of Fig. 2c, yielding hexagons with the highest degree of symmetry.

In conclusion, in this Letter we reported the observation of spontaneous pattern formation in a passive microresonator. These patterns originate from the competition of transverse diffusion, diffraction, and dispersive bandtail nonlinearities. We have also stressed the major contribution of material imperfections to the threshold of pattern formation. Modeling corroborated our interpretation of the role of the fluctuations, both as boundary conditions and as enhancement mechanisms. As precursors, these patterns are a strong indication of the possibility of observing localized states in the form of CS. Work is in progress in our laboratories in order to confirm this assertion.

Similar work performed by Taranenko and Weiss is also in progress in PTB-Braunschweig, in the frame of this project.

This work was supported in part by ESPRIT Project No. 28235 PIANOS. The authors want to acknowledge Professor L. Lugiato and Dr. I. Abram for fruitful discussions and valuable advice. M. Brambilla thanks I. Perrini for precious help with the numerics.

[1] L. Lugiato, M. Brambilla, and, A. Gatti, Adv. At. Mol. Opt. Phys. **40**, 229–306 (1998).
[2] M. Tlidi, P. Mandel, and R. Lefever, Phys. Rev. Lett. **73**, 640 (1994).
[3] M. Brambilla, L. A. Lugiato, F. Prati, L. Spinelli, and W. J. Firth, Phys. Rev. Lett. **79**, 2042 (1997).
[4] W. Firth and A. Scroggie, Phys. Rev. Lett. **76**, 1623 (1996).
[5] C. O. Weiss *et al.*, ESPRIT LTR Project No. 21112 PASS: report (1998).
[6] M. Kreuzer, W. Balzer, and T. Tschudi, Appl. Opt. **29**, 579 (1990).
[7] W. Firth, in *Proceedings of Photonics Prague'99, Prague, 1999*, SPIE Proceedings Vol. 4016 (SPIE–International Society for Optical Engineering, Bellingham, WA, 2000).
[8] L. Spinelli, G. Tissoni, M. Brambilla, F. Prati, and L. A. Lugiato, Phys. Rev. A **58**, 2542 (1998).
[9] D. Michaelis, U. Peschel, and F. Lederer, Phys. Rev. A **56**, R3366 (1997).
[10] R. Kuszelewicz, J. L. Oudar, J. C. Michel, and R. Azoulay, Appl. Phys. Lett. **53**, 22 (1988); **53**, 2138 (1988).
[11] G. Tissoni, L. Spinelli, M. Brambilla, T. Maggipinto, I. Perrini, and L. A. Lugiato, J. Opt. Soc. Am. B **16**, 2083 (1999).
[12] J. L. Oudar, R. Kuszelewicz, B. Sfez, J. C. Michel, and R. Planel, Opt. Quantum Electron. **24**, S193 (1992).
[13] R. J. Eliott, J. A. Krumhansl, and P. L. Leath, Rev. Mod. Phys. **46**, 3 (1974).